Analysis of Moiré minimization in autostereoscopic parallax displays

Lingsheng Kong,* Guang Jin, Tiancong Wang

National & Local United Engineering Research Center of Small Satellite Technology, Changchun Institute of Optics, Fine Mechanics and Physics, Chinese Academy of Sciences, Changchun, Jilin 130033, China
**lingshengkong@hotmail.com*

Abstract: In order to minimize moiré patterns in autostereoscopic parallax displays, the optical component, which is used for forming viewing zones, is analyzed with varying period and slant angle. First, horizontal-parallax autostereoscopic displays (HPAD) can be approximated as the superposition of three corresponding binary gratings. Referring to the unification of indicial equation method and Fourier analysis, a singular state and two stable moiré-free states are obtained according to the superposition of the equivalent grating of LCD and special radial grating. Two stable moiré-free states are valid for HPAD. For full-parallax autostereoscopic displays (FPAD), a special radial grid grating is introduced to simulate a 2D optical component with progressively varying period and slant angle. Similarly, two corresponding stable moiré-free states for FPAD can be used for eliminating moiré patterns.

OCIS codes: (070.0070) Fourier optics and signal processing; (050.2770) Gratings; (120.4120) Moiré techniques.

References and links

1. K. Patorski, *Handbook of the Moiré Fringe Technique* (Elsevier, 1993).
2. O. Kafri and I. Glatt, *The Physics of Moiré Metrology* (John Wiley & Sons, 1989).
3. A. T. Shepherd, "25 years of moiré fringe measurement," Precis. Eng. **1**(2), 61–69 (1979).
4. H. Takasaki, "Moiré topography," Appl. Opt. **9**(6), 1467–1472 (1970).
5. A. J. Durelli and V. J. Parks, Moiré Analysis of strain (Prentice-Hall, , 1970).
6. K. Creath and J. C. Wyant, "Moiré and fringe projection techniques," in *Optical Shop Testing*, 2nd ed. (John Wiley & Sons, 1995), 653–685.
7. I. Amidror, *The Theory of the Moiré Phenomenon*, 2nd ed (Springer, 2009).
8. J. P. Allebach, "Random nucleated halftone screen," Photogr. Sci. Eng **22**, 89–91 (1978).
9. D. Blattner, C. Chaves, G. Fleishman, and S. Roth, *RealWorld Scanning and Halftones* (Peachpit, 2004).
10. K. Mashitani, G. Hamagishi, M. Sakata, A. Yamashita, E. Nakayama,and M. Inoue, "New autostereoscopic (no-glasses) LCD image splitter displays," in 3 Dimensional Image Conf (1996), 90–95.
11. J. Hong, Y. Kim, H. J. Choi, J. Hahn, J. H. Park, H. Kim, S. W. Min, N. Chen, and B. Lee, "Three-dimensional display technologies of recent interest: principles, status, and issues [Invited]," Appl. Opt. **50**(34), H87–H115 (2011).
12. K. Taira, R. Fukushima, T. Saishu, H. Kobayashi, and Y. Hirayama, "Autostereoscopic liquid crystal display using mosaic color pixel arrangement," Proc. SPIE **5664**, 349–359 (2005).
13. T. Koike, M. Oikawa, and K. Utsugi, "Moiré reduction for integral photography," International Display Workshops (Institute of Image Information and Television Engineers of Japan and Society of Information Display, 2007), 1917–1918.
14. M. Okui, M. Kobayashi, J. Arai, and F. Okano, "Moire fringe reduction by optical filters in integral three-dimensional imaging on a color flat-panel display," Appl. Opt. **44**(21), 4475–4483 (2005).
15. L. Lipton and M. Feldman, "A new autostereoscopic display technology: the SynthaGram," Proc. SPIE **4660**, 229–235 (2002).
16. Y. Kim, G. Park, J.-H. Jung, J. Kim, and B. Lee, "Color moiré pattern simulation and analysis in three-dimensional integral imaging for finding the moiré-reduced tilted angle of a lens array," Appl. Opt. **48**(11), 2178–2187 (2009).
17. V. V. Saveljev, J.-Y. Son, B. Javidi, S.-K. Kim, and D.-S. Kim, "Moiré minimization condition in three-dimensional image displays," J. Display Technol **1**(2), 347–353 (2005).

#194789 - $15.00 USD Received 30 Jul 2013; revised 12 Sep 2013; accepted 10 Oct 2013; published 24 Oct 2013

18. V. V. Saveljev, J.-Y. Son, J.-H. Chun, and K.-D. Kwack, "About a Moiré-less condition for non-square grids," J. Display Technol **4**(3), 332–339 (2008).
19. L. S. Kong, G. Jin, T. Wang, S. Cai, X. Zhong, and K. Xu, "Parameter design of a parallax barrier based on the color moiré patterns in autostereoscopic display," Appl. Opt. **50**(34), H153–H158 (2011).
20. J. W. Goodman, Introduction to Fourier Optics (Roberts: 2005).
21. K. Patorski, S. Yokozeki, and T. Suzuki, "moiré profile prediction by using Fourier series formalism," Jpn. J. Appl. Phys. **15**(3), 443–456 (1976).
22. S. Yokozeki and K. Patorski, "moiré fringe profile prediction method and its application to fringe sharpening," Appl. Opt. **17**(16), 2541–2547 (1978).
23. D. H. Shin, E. S. Kim, and B. Lee, "Computational reconstruction of three-dimensional objects in integral imaging using lenslet array," Jpn. J. Appl. Phys. **44**(11), 8016–8018 (2005).
24. D. H. Shin, B. Lee, and E. S. Kim, "Improved Viewing Quality of 3-D Images in Computational Integral Imaging Reconstruction Based on Lenslet Array Model," ETRI Journal **28**(4), 521–524 (2006).
25. H. Choi, J. Kim, S. W. Cho, Y. Kim, J. B. Park, and B. Lee, "Three-dimensional-two-dimensional mixed display system using integral imaging with an active pinhole array on a liquid crystal panel," Appl. Opt. **47**(13), 2207–2214 (2008).
26. G. Lippmann, "La photographie integrale," C. R. Acad. Sci **146**, 446–451 (1908).
27. F. Okano, H. Hoshino, J. Arai, and I. Yuyama, "Real-time pickup method for a three-dimensional image based on integral photography," Appl. Opt. **36**(7), 1598–1603 (1997).
28. H. Hoshino, F. Okano, H. Isono, and I. Yuyama, "Analysis of resolution limitation of integral photography," J. Opt. Soc. Am. A **15**(8), 2059–2065 (1998).
29. S. H. Kaplan, "Theory of parallax barrier," J.SMPTE **59**(1), 11–21 (1952).
30. P. S. Theocaris, "Radial gratings as moiré gauges," J. Phys. E **1**(6), 613–618 (1968).
31. M. Abolhassani and M. Mirzaei, "Unification of formulation of moiré fringe spacing in parametric equation and Fourier analysis methods," Appl. Opt. **46**(32), 7924–7926 (2007).
32. V. V. Saveljev, "Orientations and branches of moiré waves in three-dimensional displays," J. Korean Phys. Soc. **57**(6), 1392–1396 (2010).

1. Introduction

The moiré phenomenon can be readily observed in the case of superimposing two periodic or quasiperiodic structures. Due to its sensitivity to the slightest displacements, variations or distortions in the overlaid structures, the moiré phenomenon is widely applied in many fields, such as strain analysis, topography and moiré metrology [1–7]. But in some other fields, such as color printing and digital image processing, it is necessary to avoid moiré patterns [7–9]. As we all know, the moiré phenomenon is unavoidable in many parallax autostereoscopic displays [10, 11], which consist of regular structures, such as LCD panel, parallax barrier, lenticular plate, pinhole array, microlens array, etc.

In previous works, two strategies were mostly used to fight against undesired moiré patterns in parallax autostereoscopic displays: avoiding moiré patterns and minimizing moiré patterns [12–18], the last of which was used in our previous works [19]. According to the superposition of the equivalent grating of LCD and the special radial grating, different corresponding predominant Fourier low-frequency terms were obtained referring to the indicial equation method and Fourier theory. Finally, the appropriate parameter of the parallax barrier (PB) can be obtained.

In order to avoid the moiré phenomenon in modern color printing, moiré minimization, which is an interesting object, is proposed by I. Amidror [7]. In this paper, moiré minimization for HPAD and FPAD is discussed, respectively. Firstly, for HPAD, with consideration of gap between LCD and PB, change of relative period is discussed in detail while viewing distance varies. Besides, the superposition of the equivalent grating of LCD and special radial grating are further discussed, and three corresponding states are given, which are singular state, angle stable moiré-free state (not sensitive for the change of slant angle) and period stable moiré-free state (not sensitive for the change of period). By using vector sum of Fundamental frequencies [7, 20–22], corresponding parameters of PB for three moiré-free states are obtained. For FPAD [23–28], a special radial grid grating, which is considered a pinhole array of progressively varying pitch and grating vector direction, is introduced in order to find corresponding predominant Fourier terms. In accordance with discussion of the superposition of the equivalent grating of LCD and special radial grid

#194789 - $15.00 USD Received 30 Jul 2013; revised 12 Sep 2013; accepted 10 Oct 2013; published 24 Oct 2013

grating, three corresponding moiré-free states can be obtained. Finally, parameters of the pinhole array, which make moiré patterns invisible in FPAD, are confirmed.

2. Analysis of moiré minimization of HPAD

2.1 Discussion of the relative period of PB for HPAD

PBs and lenticular sheets are most widely used for forming viewing zone in HPAD. In our previous work, the transition region is considered to be proper working region when the slant angle is small [19]. Now further study is carried out on HPAD based on PBs.

As we all know, there exists a certain distance between LCD and PB, so the relative period changes when the viewing distance varies from the optimum value to infinity [17]. In the following text, the relationship between relative period and viewing distance will be discussed. The principle of HPAD is illustrated in Fig. 1, and the formulas of corresponding parameter design are given as below [29]:

$$z_{optimum} = g(\frac{e+i}{i}) \tag{1}$$

$$b = Ni(\frac{z_{optimum} - g}{z_{optimum}}) \tag{2}$$

Where $z_{optimum}$ is the optimum viewing distance; g is the distance between LCD and PB; e is the average eye separation; i is the pitch of a LCD panel; N is the number of views, and b is the period of PB.

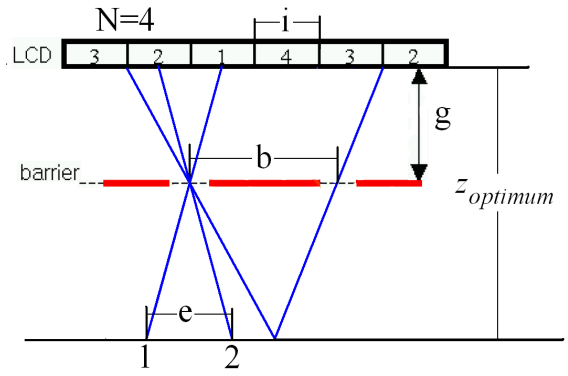

Fig. 1. The principle of multiview autostereoscopic displays based on PBs.

First, the exact definition of the relative period is given. As shown in Fig. 2, we set up a standard as bellow: for HPAD, one image is observed at an arbitrary distance z; the other image is obtained at infinity while the period of PB equals b`.

#194789 - $15.00 USD Received 30 Jul 2013; revised 12 Sep 2013; accepted 10 Oct 2013; published 24 Oct 2013

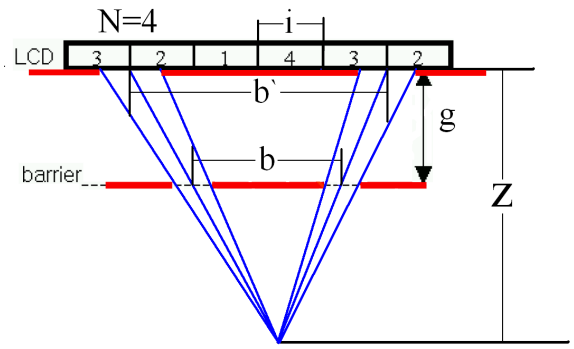

Fig. 2. The interpretation of the relative period of PBs.

Apparently, both images are identical (namely two kinds of superposition are equivalent for viewers), and we define that the relative period of PB equals b` in this case. The relative period $b`$ is determined by considering similar triangles.

$$b` = \frac{z}{z-g} b \tag{3}$$

Where z is the viewing distance; g is the distance between LCD and PB; b is the period of PB, and $b`$ is the relative period. Based on Eq. (3), we conclude that the relative period of PB equals Ni in the optimum viewing distance. Similarly, when the viewing distance equals infinity, the relative period of PB equals $Ni(\frac{z_{optimum}-g}{z_{optimum}})$ (namely b).

Usually, the value of g approximates 1 mm while the optimum viewing distance z is far greater than 1 mm. Thus, there exists slight change for the relative period of PB when z varies from the optimum value to infinity. However, the slight change of the relative period cannot be neglected when the superposition of LCD and PB falls into the singular state. Therefore, the parameters of PB must be away from the singular state. Similarly, the singular state should be avoided for FPAD.

2.2 Analysis of moiré minimization of the superposition of the equivalent grating of LCD and special radial grating

In our previous work [19], the superposition of the special radial grating and the equivalent binary grating of LCD is consistent with Fig. 2 in [17], so we quoted angle 26.61°and discussed the circumstances of being less than 26.61°. In this paper, all the regions will be discussed according to the unification of indicial equation method and Fourier analysis method [30, 31]. First, the opening ratio of gratings only influences the intensity profile of moiré patterns [7]. Thus, for simplicity, LCD is represented as a 2D binary grating with an opening ratio of 1/3 as shown in Fig. 3(a). The width of the pixel (P_1) and subpixel (P) of the LCD has the relationship of $P_1 = 3P$. The special radial grating is shown in Fig. 3(b). The superposition of the equivalent grating of LCD and special radial grating is shown in Fig. 4. According to the symmetric relationship, the slant angle θ varies from 0°to 45° [17]. Similarly, along the line A, moiré patterns change gently when the period of PB varies. In order to find α value, the superposition in Fig. 4 will be further discussed.

#194789 - $15.00 USD Received 30 Jul 2013; revised 12 Sep 2013; accepted 10 Oct 2013; published 24 Oct 2013

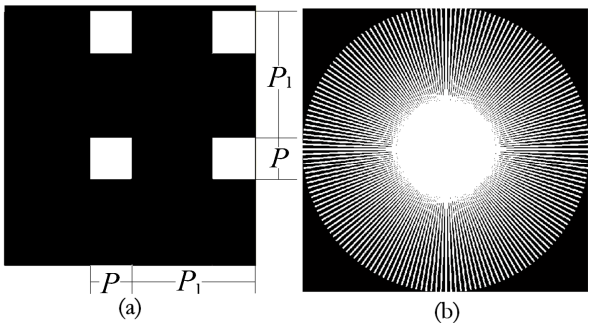

Fig. 3. (a) The equivalent grating of LCD (b) The special radial grating.

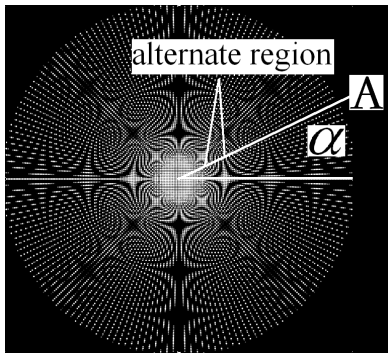

Fig. 4. Superposition of the equivalent grating of LCD and special radial grating.

Firstly, star patterns in the region, where the slant angle is near 0°, were discussed completely and the corresponding Fourier terms were given [19]. Secondly, for the star patterns in the region, where the slant angle is near ± 45°, it is easy to figure out that there exist parallel line families with slant angles ± 45°, which are superposed on the special radial grating to form the star patterns in the region near ± 45°. The equivalent grating of LCD can be expressed as $T_1(x,y) = \sum_{r=-\infty}^{r=\infty} a_r \cos(2\pi r x / P_1) \times \sum_{h=-\infty}^{h=\infty} c_h \cos(2\pi h y / P_1)$ and Fourier terms with the slant angle of ± 45° in $T_1(x, y)$ could be found [20–22]. Based on Fourier theory, when $r = \pm h$, partial sum terms in $T_1(x, y)$ correspond to parallel line families with slant angles ± 45°. Figure 5 shows the corresponding parallel line families in the image domain when $r = \pm h$ and the Fourier vector diagram (For simplicity, there are only two fundamental frequency terms in Fig. 5(b). $\left|\vec{f}_1\right|$ and $\left|\vec{f}_2\right|$ are the transverse and longitudinal fundamental frequencies of the equivalent binary grating of LCD respectively, $\left|\vec{f}_2\right| = \left|\vec{f}_1\right|$). Here, the period $P`$ of the corresponding parallel line family equals $0.707P_1$.

#194789 - $15.00 USD Received 30 Jul 2013; revised 12 Sep 2013; accepted 10 Oct 2013; published 24 Oct 2013

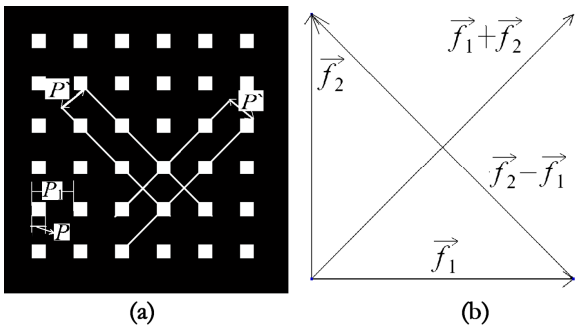

Fig. 5. (a) The equivalent grating of LCD (b) Vector sum of Fourier frequencies.

According to the comparison of our work and refs [5] [7], we can conclude that star patterns near 0°accord with (1,0,1)-moiré(namely wave 1 in [32]) while star patterns near 45°and (1,1,1)-moiré(namely wave 11 in [32]) are consistent. In the following, states in the case of different superpositions will be discussed by the vectorial difference.

It is easy to figure out that the centers of the star regions correspond to singular states of HPAD. The period of predominant moiré patterns approaches infinity when superposition of LCD and PB falls in the singular state, and there is no degradation in image quality. However, the tiny error of the period P_2 of PB caused by machining imperfection or errors of slant angle occurring during assemble and adjustment will generate new visible moiré patterns. In addition, small change of viewing distance of human eyes will also lead to the relative period change. Thus, the singular state cannot be regarded as the working state and should be avoided. The PB parameters corresponding to the singular state are shown in Table 1:

Table 1. Parameters of PB in the singular state

Singular state	
θ (°)	P_2
0	$3MP, M \in N$
45	$0.707 * 3MP, M \in N$

For (1, 0, 1)-moiré, there exist transition regions, where moiré patterns are not sensitive to small changes of slant angle [19]. In similar manner, there also exist transition regions for (1, 1, 1)-moiré. Here all the transition regions are defined as angle stable moiré-free state. The PB parameters corresponding to angle stable moiré-free state are shown as follows in Table 2:

Table 2. Parameters of PB in the angle stable state

Angle stable moiré-free state	
θ (°)	P_2
$0 < \theta < \alpha$	$4.5MP / \cos(\theta), M \in N$
$\alpha < \theta < 45^{\circ}$	$P_2 = 4.5 * 0.707MP / \cos(\frac{\pi}{4} - \theta), M \in N$

Obviously, moiré patterns along the line A in Fig. 4 are not sensitive to the small period change, which is called period stable moiré-free state. Firstly, the physical meaning of the angle α is analyzed. Seen from Fig. 4, (1, 0, 1)-moiré is predominant when slant angle is less than α, and (1, 1, 1)-moiré becomes predominant when slant angle is greater than α. Along the line A, two kinds of moiré patterns alternately act as the predominant moiré patterns when the period of PB increases. Because the two kinds of moiré patterns vary periodically

#194789 - $15.00 USD Received 30 Jul 2013; revised 12 Sep 2013; accepted 10 Oct 2013; published 24 Oct 2013

with the period of PB increasing, it is enough to discuss the first repeat region instead of the whole region in Fig. 4. The Fourier vector sum diagram is shown in Fig. 6, where the fundamental frequency of PB is $\vec{f}_p$. When $\left|\vec{f}_p\right| = \left|\vec{f}_1\right|\cos(\alpha)$, (1, 0, 1)-moiré is predominant and achieves an extreme value of $\left|\vec{f}_1\right|\sin(\alpha)$; when $\left|\vec{f}_p\right| = \left|\vec{f}_1 + \vec{f}_2\right|\cos(\alpha) = \sqrt{2}\left|\vec{f}_1\right|\cos(\pi/4-\alpha)$, (1, 1, 1)-moiré is predominant and achieves an extreme value of $\sqrt{2}\left|\vec{f}_1\right|\sin(45-\alpha)$. In this alternate region, the period of predominant moiré patterns decreases firstly and increases afterwards. Therefore, the variation of predominant moiré patterns' period is minimal when the slant angle equals α . Thus, a standard is built up that the slant angle equals α when the two extreme values equal. Based on this standard, the following equations are given:

$$\left|\vec{f}_1\right|\sin(\alpha) = \sqrt{2}\left|\vec{f}_1\right|\sin(45-\alpha) \tag{4}$$

Thus,

$$\tan(\alpha) = 0.5, \alpha = 26.565^{\circ}$$

The value of α consists with the result in [32]. Next, variations of periods of two kinds of moiré patterns are shown respectively in Fig. 7(a) when the fundamental frequency $\left|\vec{f}_p\right|$ of PB varies from $\left|\vec{f}_1\right|\cos(\alpha)$ to $\sqrt{2}\left|\vec{f}_1\right|\cos(\pi/4-\alpha)$. The x-axis represents the value of $\left|\vec{f}_p\right|$ while the y-axis represents the frequency f_m of two kinds of moiré patterns. The thin line represents the frequency of (1, 0, 1)-moiré and the thick line represents the frequency of (1, 1, 1)-moiré. The maximal values of the two kinds of moiré patterns are located on point C and point D respectively in Fig. 6, while the two extreme values equal to each other. At the intersection point O, two kinds of moiré patterns have the same strength.

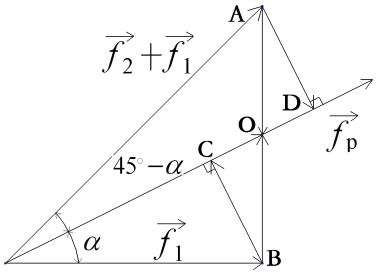

Fig. 6. Vector sum of Fourier fundamental frequencies of LCD and PB.

From the discussion mentioned above, in the CO region, (1, 0, 1)-moiré is predominant, and in OD region (1, 1, 1)-moiré acts dominantly. The frequencies F_m of actual predominant moiré patterns are shown in Fig. 7 (b) (the y-axis represents the frequency F_m of predominant moiré patterns).

#194789 - $15.00 USD Received 30 Jul 2013; revised 12 Sep 2013; accepted 10 Oct 2013; published 24 Oct 2013

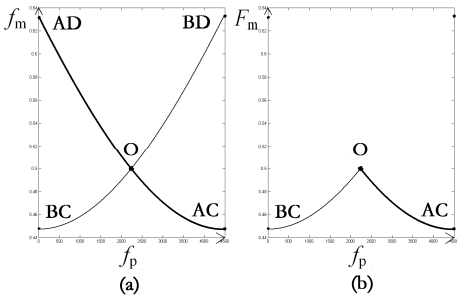

Fig. 7. (a) Frequencies of (1, 0, 1)-moiré and (1, 1, 1)-moiré (b) Frequencies of predominant moiré patterns.

It is easy to figure out that the period of predominant moiré patterns fluctuates the least with the period of PB varies in the period stable moiré-free state.

The superposition of the equivalent gratings of LCD and PB is simulated numerically for three moiré-free states in Fig. 8. First, the superpositions in Figs. 8(a), 8(b), 8(c), 8(d) and 8(e) indicate that a singular state is very unstable and very sensitive to any slight deviation in the angle or in the period of PB. Second, for superposition around the angle stable moiré-free state, moiré patterns in Figs. 8(f), 8(g) and 8(h) change slowly with the variation of slant angle of PB. Third, moiré patterns in Figs. 8(i), 8(j) and 8(k) show no violent variation exists when the period of PB varies.

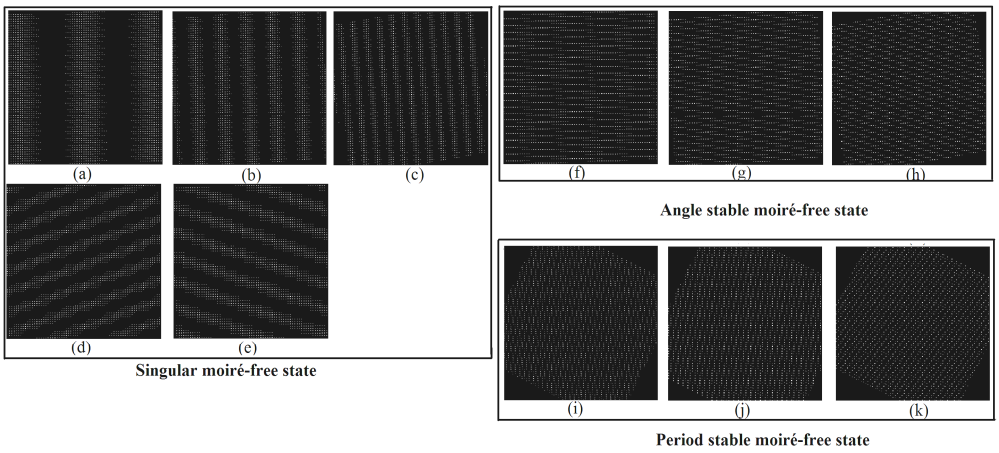

Fig. 8. (a) θ=2° , $P_2 = 3P$ (b) θ=5° , $P_2 = 3P$ (c) θ=10° , $P_2 = 3P$ (d) θ=2° , $P_2 = 2.7P$ (e) θ=2° , $P_2 = 3.3P$ (f) θ=2° , $P_2 = 4.5P$ (g) θ=5° , $P_2 = 4.5P$ (h) θ=10° , $P_2 = 4.5P$ (i) θ=26.565° , $P_2 = 2.4P$ (j) θ=26.565° , $P_2 = 3P$ (k) θ=26.565° , $P_2 = 3.6P$.

For HPAD, parameters of PB must be away from a singular state. The period of predominant moiré patterns must be less than 1 mm to make it invisible for human eyes when parameters of PB fall in the angle stable moiré-free state [7, 19]. (1, 0, 1)-moiré and (1, 1, 1)-moiré are both invisible for human eyes when the parameters of PB fall in the period stable moiré-free state.

3. Analysis of moiré minimization of FPAD

FPAD forms the viewing zone by use of optical components with 2D structures, such as pinhole array, microlens array etc [23–28]. Here, the corresponding optical components of FPAD are regarded as 2D binary grating in Fig. 9 (a). Similarly, the period P_3 and slant angle θ of 2D binary grating are variable in quantity. The opening ratio of the grating does not

#194789 - $15.00 USD Received 30 Jul 2013; revised 12 Sep 2013; accepted 10 Oct 2013; published 24 Oct 2013

influence the period and slant angle of moiré patterns, so the opening ratio of 2D binary grating is set to 1/3 arbitrarily. Besides, the equivalent binary grating of LCD is a 2D binary grating. Thus, FPAD can be considered as the supposition of two 2D binary gratings. In order to analyze the superposition of the equivalent binary grating of LCD and 2D binary grating with varying period and slant angle, a special radial grid grating is introduced as shown in Fig. 9(b). Seen from the local region in Fig. 9(b), it represents a 2D binary grating with progressively varying period and slant angle.

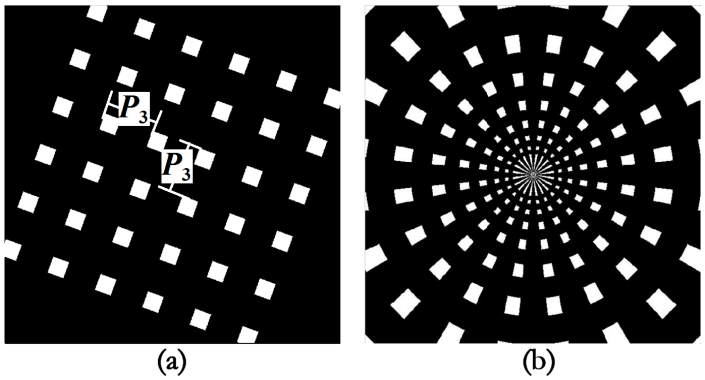

Fig. 9. (a) The equivalent 2D binary grating (b) The special radial grid grating.

Superposition of special radial grid grating and the equivalent binary grating of LCD is shown in Fig. 10. It is easy to figure out that Figs. 4 and 10 have similar patterns. The star patterns in Fig. 10 are located in the same place as the previous star patterns in Fig. 4, but the shape is more complicated and different from the previous ones. Obviously, star patterns in Fig. 4 have four horns while star patterns in Fig. 10 have eight horns.

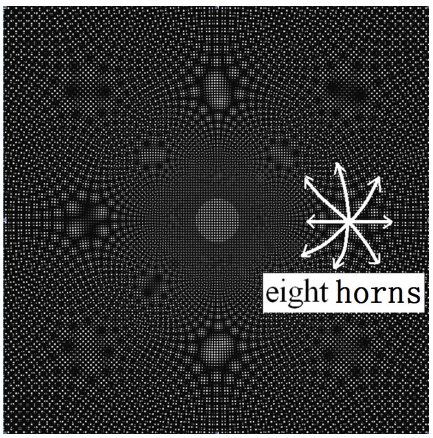

Fig. 10. Superposition of equivalent grating of LCD and special radial grid grating.

For the sake of analyzing moiré patterns in Fig. 10, the special radial grid grating is resolved into the product of radial grating and circle grating, as shown in Fig. 11.

#194789 - $15.00 USD Received 30 Jul 2013; revised 12 Sep 2013; accepted 10 Oct 2013; published 24 Oct 2013

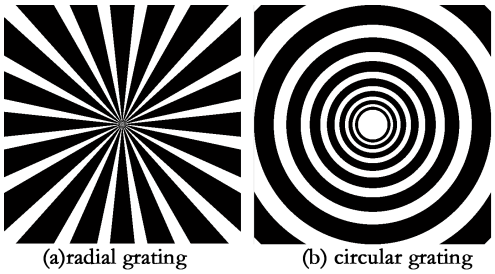

Fig. 11. Radial and circular gratings which are resolved from special radial grid grating.

According to Refs [17, 19, 30], the radial grating in Fig. 11(a) is equivalent to a line grating with varying period and slant angle. In a like manner, the circular grating in Fig. 11(b) also can be considered as a line grating with varying period and slant angle. Apparently, at the same location in Figs. 11 (a) and 11(b), corresponding periods of the local equivalent line gratings are equal while their orientations are perpendicular. The superposition of the resolved radial grating and the equivalent binary grating of LCD is shown in Fig. 12(a). Because the opening ratio of the grating only influences the profiles of moiré patterns, Fig. 12(a) coincides with Fig. 4.

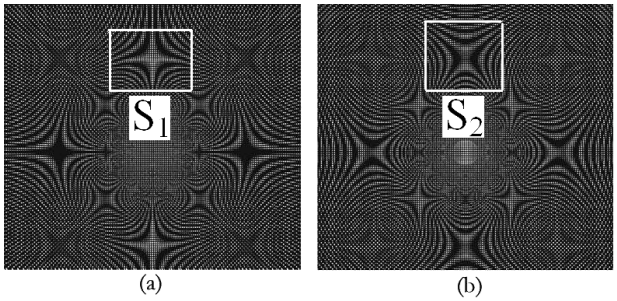

Fig. 12. (a) Superposition of equivalent grating of LCD and radial grating (b) Superposition of equivalent grating of LCD and circular grating.

Superposition of circular grating and the equivalent binary grating of LCD is shown in Fig. 12 (b). As shown in Figs. 12(a) and 12(b), two types of star patterns have the same location and numbers of horns (namely four horns), but the horns' orientations of two figures are different. However, star pattern S_1 become the same as star pattern S_2 after it rotated 45°。 seen from Fig. 12,The local equivalent line gratings of circular grating and radial grating have the same period and opening ratio but perpendicular to each other, so it is very reasonable to conclude that the star patterns S_1 has the same shape as the star patterns S_2 in Fig. 12.

It's easy to see that the star patterns in Figs. 12(a) and 12(b) have four horns, but the star patterns in Fig. 10 have eight horns. So the patterns in Fig. 10 can be considered as the results of the coactions of Figs. 12(a) and 12(b). Here, we interpret the coactions by use of an example. As shown in Fig. 13, two 2D gratings are superposed and the square moiré patterns are formed, which is consistent with star patterns near 0°in Fig. 10. 2D grating 1 can be resolved into the product of 1D grating 1 and 1D grating 2, while 2D grating 2 can be resolved into the product of 1D grating 3 and 1D grating 4. Apparently, the product of 1D grating 1 and 1D grating 3 is moiré pattern 1, while the product of 1D grating 2 and 1D grating 4 is moiré pattern 2. Square moiré patterns also can be resolved in the product of moiré pattern 1 and 2. With the same manner, eight horns in Fig. 10 are the coactions of two four-horn patterns (namely S_1 and S_2).

#194789 - $15.00 USD Received 30 Jul 2013; revised 12 Sep 2013; accepted 10 Oct 2013; published 24 Oct 2013

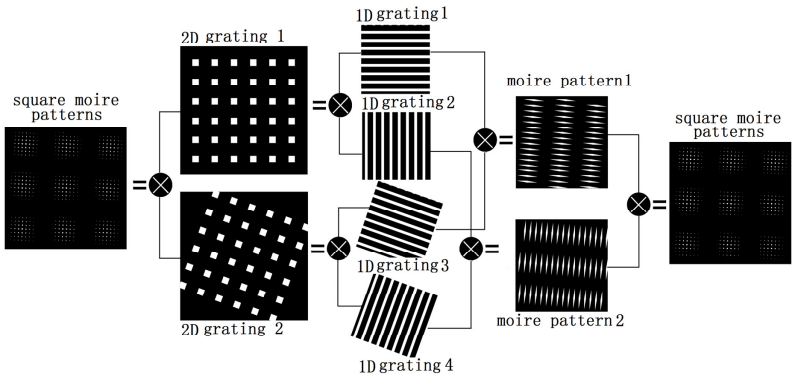

Fig. 13. Interpretation of the coactions of Figs. 12(a) and 12(b).

Combining the conclusions of HPAD, we put out the inferences on FPAD as follows:

1. When the slant angle of 2D optical component is greater than 0 but less than α, two types of predominant moiré patterns exist. One is (1, 0, 1, 0)-moiré just like the one in HPAD. The other is (0, 1, 0, 1)-moiré with a perpendicular slant angle, same period and intensity profile as (1, 0, 1, 0)-moiré.

2. When the slant angle of 2D optical component is greater than α but less than 45°, two types of predominant moiré patterns also exist. One is (1, 1, 1, 0)-moiré just like the one in HPAD. The other is (1, −1, 0, −1)-moiré with a perpendicular slant angle, and the same period and intensity profile as (1, 1, 1, 0)-moiré.

Same three states, which are the singular state, period stable moiré-free state and angle stable moiré-free state, are also found in FPAD. Superposition of two equivalent 2D gratings is simulated numerically for three moiré-free states in Fig. 14. Similar as the analysis of Fig. 8, comparisons of three different states are given respectively.

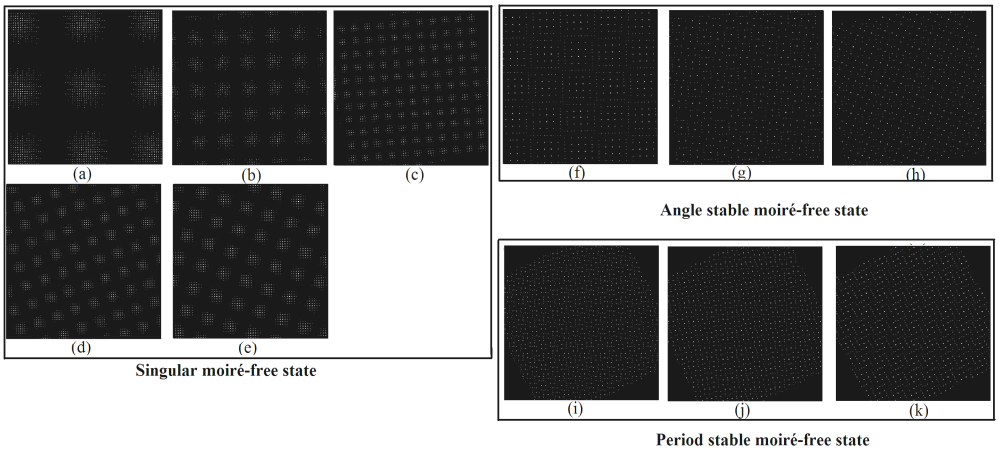

Fig. 14. (a) θ=2° , $P_3 = 3P$ (b) θ=5° , $P_3 = 3P$ (c) θ=10° , $P_3 = 3P$ (d) θ=2° , $P_3 = 2.7P$ (e) θ=2° , $P_3 = 3.3P$ (f) θ=2° , $P_3 = 4.5P$ (g) θ=5° , $P_3 = 4.5P$ (h) θ=10° , $P_3 = 4.5P$ (i) θ=26.565° , $P_3 = 2.4P$ (j) θ=26.565° , $P_3 = 3P$ (k) θ=26.565° , $P_3 = 3.6P$.

Generally, FPAD and HPAD have the same design for optical components.

#194789 - $15.00 USD Received 30 Jul 2013; revised 12 Sep 2013; accepted 10 Oct 2013; published 24 Oct 2013

4. Conclusions

In conclusion, for HPAD, superposition of the equivalent grating of LCD and special radial grating is analyzed completely referring to unification of indicial equation method and Fourier analysis. Three states, which are singular state, period stable moiré-free state and angle stable moiré-free state, are obtained through moiré minimization analysis of HPAD. Moiré patterns can be avoided in the case of period and angle stable moiré-free states while the singular state is not good enough for fighting against moiré patterns in HPAD.

For FPAD, we propose a model of special radial grid grating, which is considered as 2D optical components of progressively varying pitch and grating vector direction. Similarly, the superposition of the equivalent grating for LCD and special radial grid grating is analyzed referring to the indicial equation method and Fourier theory. Three corresponding states, which are consistent with states for HPAD, are obtained for FPAD as well.

#194789 - $15.00 USD Received 30 Jul 2013; revised 12 Sep 2013; accepted 10 Oct 2013; published 24 Oct 2013